

Research Article

CCR2-dependent Gr1^{high} monocytes promote kidney injury in shiga toxin-induced hemolytic uremic syndrome in mice

Judith-Mira Pohl¹, Julia K. Volke¹, Stephanie Thiebes¹,
Alexandra Brenzel¹, Kerstin Fuchs², Nicolas Beziere²,
Walter Ehrlichmann², Bernd J. Pichler², Anthony Squire¹, Faikah Gueler³
and Daniel R. Engel¹ 

¹ Institute of Experimental Immunology and Imaging, University Duisburg-Essen and University Hospital Essen, Essen, Germany

² Werner Siemens Imaging Center, Department of Preclinical Imaging and Radiopharmacy, Eberhard Karls University of Tuebingen, Tuebingen, Germany

³ Department of Nephrology and Hypertension, Hannover Medical School, Hannover, Germany

The hemolytic uremic syndrome (HUS) is a life-threatening disease of the kidney that is induced by shiga toxin-producing *E.coli*. Major changes in the monocytic compartment and in CCR2-binding chemokines have been observed. However, the specific contribution of CCR2-dependent Gr1^{high} monocytes is unknown. To investigate the impact of these monocytes during HUS, we injected a combination of LPS and shiga toxin into mice. We observed an impaired kidney function and elevated levels of the CCR2-binding chemokine CCL2 after shiga toxin/LPS- injection, thus suggesting Gr1^{high} monocyte infiltration into the kidney. Indeed, the number of Gr1^{high} monocytes was strongly increased one day after HUS induction. Moreover, these cells expressed high levels of CD11b suggesting activation after tissue entry. Non-invasive PET-MR imaging revealed kidney injury mainly in the kidney cortex and this damage coincided with the detection of Gr1^{high} monocytes. Lack of Gr1^{high} monocytes in *Ccr2*-deficient animals reduced neutrophil gelatinase-associated lipocalin and blood urea nitrogen levels. Moreover, the survival of *Ccr2*-deficient animals was significantly improved. Conclusively, this study demonstrates that CCR2-dependent Gr1^{high} monocytes contribute to the kidney injury during HUS and targeting these cells is beneficial during this disease.

Keywords: CCR2 · Gr1^{high} monocytes · HUS · Kidney injury · Shiga toxin



Additional supporting information may be found in the online version of this article at the publisher's web-site

Introduction

Shiga-toxin (Stx) –producing enterohaemorrhagic *E.coli* (STECs) have been implicated in serious outbreaks of the hemolytic uremic syndrome (HUS), a life-threatening disease characterized

Correspondence: Prof. Daniel R. Engel
e-mail: engel@immunodynamics.de

by microangiopathic haemolytic anaemia, thrombocytopenia and acute kidney injury [1]. In this disease, Stx traverses the intestinal epithelium and binds to the glycolipid globotriaosylceramide (Gb3) on endothelial cells causing severe vascular damage [2]. The animal model that mimics STEC-HUS is induced by the injection of LPS and Stx into mice [3–6]. Since Gb3 is highly expressed in the renal microvasculature, the Stx-dependent endothelial damage causes acute kidney injury and reduces the glomerular filtration capacity [7, 8]. Among other, damage to the renal endothelium is characterized by increased serum levels of blood urea nitrogen (BUN) [8, 9]. Moreover, endothelial damage induces binding of platelets to exposed subendothelial collagen, which further induces the recruitment of leukocytes to the site of vascular injury [10]. Moreover, neutrophil gelatinase-associated lipocalin (NGAL) is a transient tubular damage marker that indicates injury of proximal tubular epithelial cells. However, a therapy against this severe disease is still elusive, thus further interventional studies are required to delineate the mechanism relevant during HUS.

The kidney harbors a dense network of myeloid cells, such as macrophages and dendritic cells [11, 12]. In homeostatic and inflammatory conditions, these cells are present throughout the interstitial and mesangial spaces of the entire kidney [11]. Macrophages have been shown to undergo local proliferation during inflammation in the kidney [13]. Moreover, monocytes have been shown to differentiate into macrophages after leaving the blood stream and entering the kidney [14]. Two subsets of blood monocytes have been identified previously, which can be subdivided by their differential expression of the surface molecule Gr1 and the chemokine receptor CCR2 [15, 16]. During HUS, there is evidence for increased expression of monocyte-recruiting chemokines, such as CCL2, CCL3 and CCL5 and upregulation of the corresponding receptors, namely CCR1, CCR2 and CCR5 has been shown [5, 17–19]. Major changes in the composition of monocytes in the blood has been observed during HUS and histological studies of HUS biopsy specimens showed the presence of monocytes in the glomeruli [18, 20]. These data suggest an important role of chemokine-dependent recruitment of monocytes during HUS. In this study, we have investigated the specific contribution of Gr1^{high} monocytes during HUS by employing mice deficient for CCR2.

Results

Acute kidney injury is associated with increased chemokine expression

To investigate the kidney damage in mice after inducing HUS, we intravenously injected a combination of Stx and LPS into mice and assessed the level of kidney function by measuring blood urea nitrogen (BUN). We observed elevated levels of BUN in the serum (Fig. 1A), increased expression of the kidney injury marker-1 (KIM-1) (Fig. 1B) and elevated tubular expression of neutrophil gelatinase-associated lipocalin (NGAL) in the kidney of these mice (Fig. 1C), thereby indicating acute kidney injury. Next, we ana-

lyzed the levels of the monocyte-recruiting chemokines CCL2, CCL3, CCL4 and CCL5 in the supernatant of homogenized kidneys. We detected elevated levels of these chemokines in kidney homogenates of Stx/LPS-treated mice (Fig. 2) suggesting that a chemokine-dependent recruitment of monocytes contributes to the reduced kidney function.

Next, we characterized the phenotype of renal macrophages (F4/80⁺Gr1^{low}) and monocytes (F4/80⁺Gr1^{high}) after injection of Stx/LPS. We found that Gr1^{low} macrophages and Gr1^{high} monocytes showed differential expression of CX₃CR1, MHC class II and CD11c, whereas MerTK and CD64 were similarly expressed (Supporting Information Fig. 1A and B). Thus, the following phenotypes could be determined: Gr1^{low} macrophages (CX₃CR1^{high} MerTK⁺ MHC class II^{high} CD64^{high} CD11c^{low} Ly6C⁻ Ly6G⁻); Gr1^{high} monocytes (CX₃CR1^{low} MerTK⁺ MHC class II⁻ CD64^{high} CD11c⁻ Ly6C⁺ Ly6G⁻).

We further determined the abundance of Gr1^{low} macrophages and Gr1^{high} monocytes during HUS. We found a strong increase of Gr1^{high} monocytes on day 1 post Stx/LPS injection (Fig. 3A and B). We also observed that these cells highly expressed the integrin CD11b (Fig. 3C) suggesting that these cells are activated during HUS. In contrast, Gr1^{low} macrophages were less frequent on day 2 post Stx/LPS, but returned to the steady levels on day 3 (Fig. 3A and B). To investigate whether this increase can be explained by differentiation of Gr1^{high} monocytes into Gr1^{low} macrophages, we transferred CD45.1⁺ Gr1^{high} monocytes (Supporting Information Fig. 2) at the day of disease induction into CD45.2 recipients. We detected adoptively transferred Gr1^{high} monocytes on day 1 (Supporting Information Fig. 3A), whereas CD45.1⁺ Gr1^{low} macrophages were barely detectable on day 1 and day 3 (Supporting Information Fig. 3B). These data suggest that the increase of Gr1^{low} macrophages on day 3 might be due to other mechanisms beyond differentiation of Gr1^{high} monocytes. To further investigate whether the return of Gr1^{low} macrophages on day 3 can also be explained by self-renewal, we analyzed the incorporation of BrdU during the course of the disease. We found that some Gr1^{low} macrophages incorporated BrdU on day 3 demonstrating their proliferative capacity after Stx/LPS injection (Supporting Information Fig. 3C).

Non-invasive in vivo imaging and microscopy reveal kidney injury and Gr1^{high} monocytes in the cortex

We then localized the kidney injury and Gr1^{high} monocytes in the kidney by non-invasive in vivo imaging and microscopy. We employed positron emission tomography (PET) and co-registered magnet resonance (MR) images after injection of [⁶⁴Cu]NOTA-glycoprotein VI (GPVI)-Fc tracer [21, 22] to detect exposed subendothelial collagen after endothelial injury in the kidney. We found enhanced uptake of this tracer in the kidney after Stx/LPS injection (Fig. 4A and B) demonstrating endothelial damage and identifying a novel non-invasive imaging technique to score endothelial kidney injury during HUS. We also observed accumulation of the tracer in the liver, which is a common phenomenon for

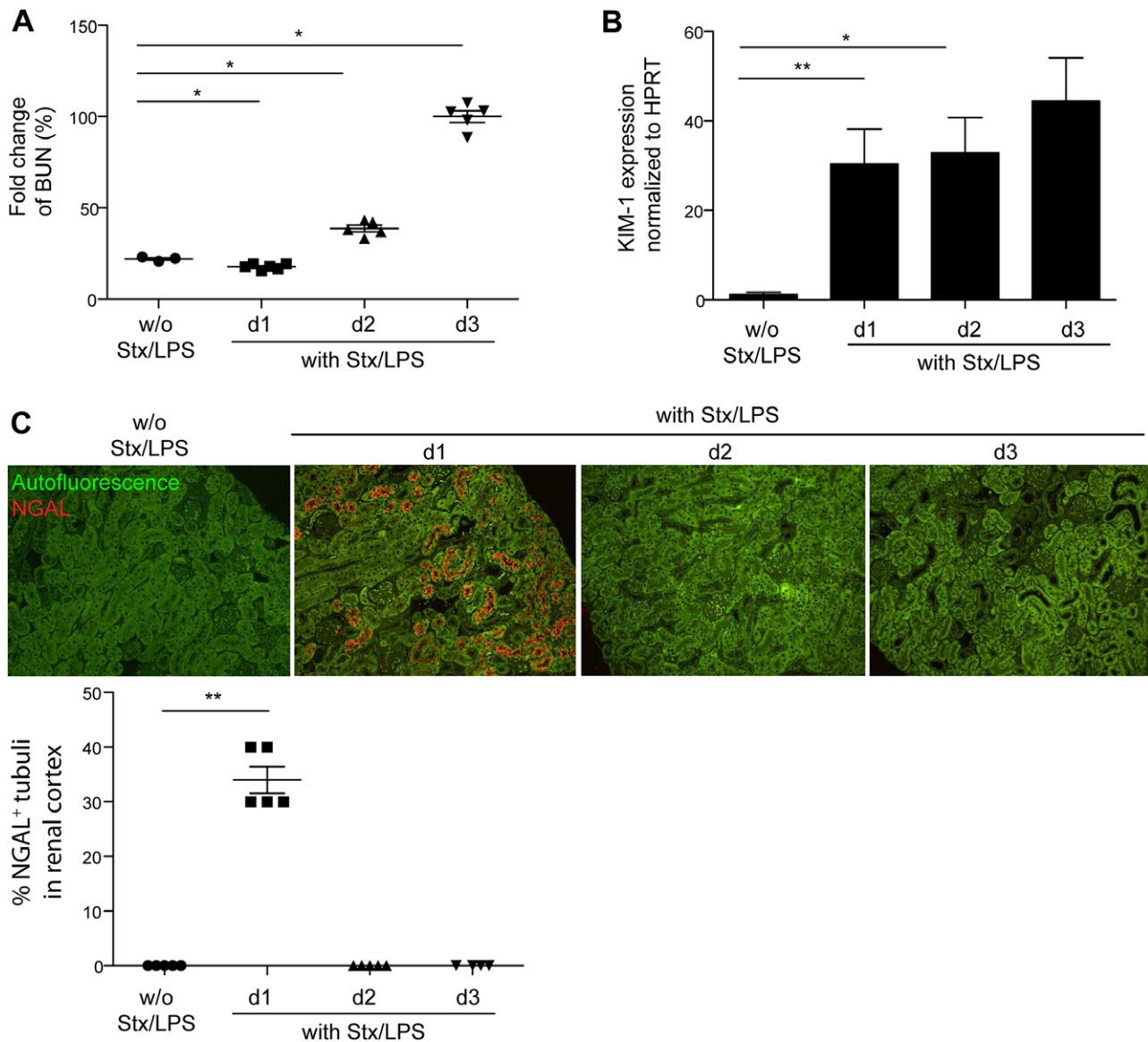


Figure 1. Increased kidney injury in mice after Stx/LPS injection. (A) BUN levels in the blood were analyzed on day 1 to day 3 after Stx/LPS injection. (B) Expression of the Kidney Injury Molecule-1 (KIM-1) in kidneys was determined by quantitative RT-PCR and the expression was normalized to the house keeping gene HPRT. Samples were assayed in duplicates. (C) The expression of NGAL was determined by staining histological sections at the time points indicated. The quantitative analysis indicates the percentage of NGAL⁺ tubuli in the renal cortex. Data in (A) and (B) are representative of five independent experiments with $n = 3-6$. The KIM values from untreated mice (w/o Stx/LPS) and three days after Stx/LPS injection were determined in two independent experiments. Data in (C) represent a single experiment with a group size of $n = 4-5$ mice. Results are given as mean \pm SEM and symbols represent a single mouse. p -value was calculated with Mann-Whitney test. * $p < 0.05$; ** $p < 0.01$. d = day; BUN = blood urea nitrogen; KIM = Kidney Injury Molecule, NGAL = neutrophil gelatinase-associated lipocalin.

⁶⁴Cu-labelled tracers due to the trans-chelation of copper to liver enzymes [23]. Ex vivo autoradiography revealed a strong tracer-signal in the cortex of Stx/LPS injected animals (Fig. 4A, lower right image). To analyze whether this accumulation of the tracer in the cortex is associated with the infiltration of Gr1^{high} monocytes on day 1 post Stx/LPS injection, we localized these cells in the kidney by histology. We found numerous Gr1^{high} monocytes particularly in the renal cortex (Fig. 5A and B), thereby suggesting that the appearance of Gr1^{high} monocytes in the renal cortex may cause the kidney injury.

Targeting CCR2-dependent Gr1^{high} monocytes ameliorates kidney injury

To investigate whether Gr1^{high} monocytes contribute to the development of HUS, we assessed the proinflammatory cytokine milieu in the kidney, the kidney damage by measuring BUN, the survival and the expression of NGALs, in *Ccr2*-deficient mice. We found reduced abundance of Gr1^{high} monocytes in the kidney in *Ccr2*-deficient mice, whereas Gr1^{low} macrophages were unchanged (Fig. 6A). The absence of Gr1^{high} monocytes

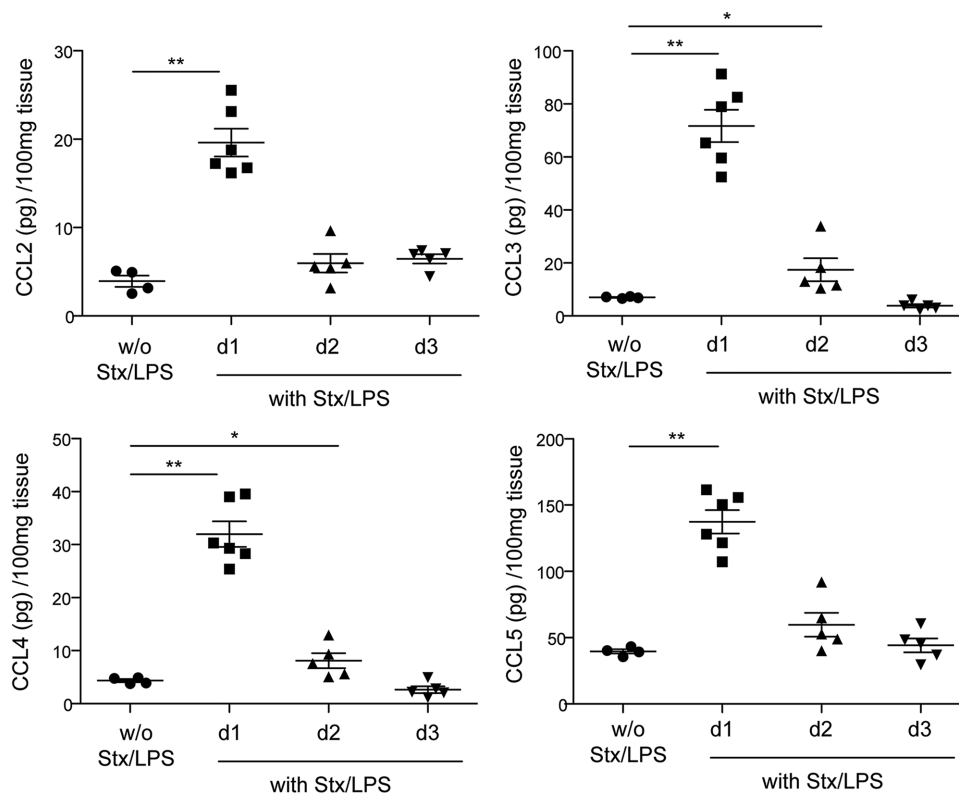


Figure 2. Elevated levels of monocyte-recruiting chemokines after Stx/LPS injection. The amount of CCL2, CCL3, CCL4 and CCL5 was determined in the supernatants of mechanically homogenized kidneys of untreated mice (w/o Stx/LPS) and on day 1 to day 3 after Stx/LPS injection. Results are from a single experiment with four to six mice and given as mean \pm SEM. Symbols represent a single mouse. *p*-value was calculated with Mann-Whitney test. **p* < 0.05; ***p* < 0.01. d = day.

in *Ccr2*-deficient animals significantly reduced the BUN levels in the serum (Fig. 6B) and the survival was significantly improved (Fig. 6C). Although only slightly increased in comparison to the healthy controls, we found that IL-1b and IL-6 were significantly decreased on day 3 (Supporting Information Fig. 4) indicating that the inflammatory response might be ameliorated in the absence of Gr1^{high} monocytes between day 1 and day 3. Moreover, we detected reduced expression of NGAL on day 1 (Fig. 6D). These data demonstrate that CCR2-dependent Gr1^{high} monocytes are critical for the development of HUS.

Discussion

Monocytes are critical inducers of kidney diseases and targeting the recruitment of these cells prevents inflammation and disease induction [12, 24–26]. The recruitment of monocytes is mediated by chemokines and their receptors and targeting these molecules has been shown beneficial against inflammation and disease progression [25, 27–31]. During HUS, there is evidence for increased expression of monocyte-recruiting chemokines [5, 17, 18] and upregulation of their receptors has been observed [19, 20]. We found an increased expression of the chemokines CCL2, CCL3, CCL4 and CCL5 during HUS. We also found that the expression of these chemokines in the kidney coincided with the detection of

Gr1^{high} monocytes. The presence of this monocyte subset is mainly regulated by CCR2, the receptor that binds some of the aforementioned chemokines by a mechanism that enables the emigration of Gr1^{high} monocytes from the bone marrow [16, 32, 33]. We found that an impaired abundance of Gr1^{high} monocytes in *Ccr2*-deficient animals reduce Stx-induced kidney damage and improved the survival.

The presence of Gr1^{high} monocytes has previously been associated with inflammation, tissue injury and reduced functionality of the kidney [12, 25]. Moreover, Gr1^{high} monocytes are efficient producers of inflammatory molecules that might contribute to the kidney injury and the development of HUS. As the kidney injury marker NGAL and BUN were strongly decreased in *Ccr2*-deficient animals, Gr1^{high} monocytes seemed to be directly involved in kidney damage during HUS. Microscopy revealed the presence of Gr1^{high} monocytes in the kidney cortex, which harbors the main functional units within the kidney, the glomeruli. We also detected an increased uptake of the tracer [⁶⁴Cu]NOTA-GPVI-Fc within the kidney cortex by PET-MR imaging suggesting that Gr1^{high} monocytes within the renal glomeruli are directly involved in the glomerular damage and increased BUN levels.

Gr1^{high} monocytes highly expressed the integrin CD11b, which indicates cellular activation and binding to the adhesion molecule ICAM-1 expressed on endothelial cells. Indeed, ICAM-1 was previously shown to be upregulated on endothelial cells after

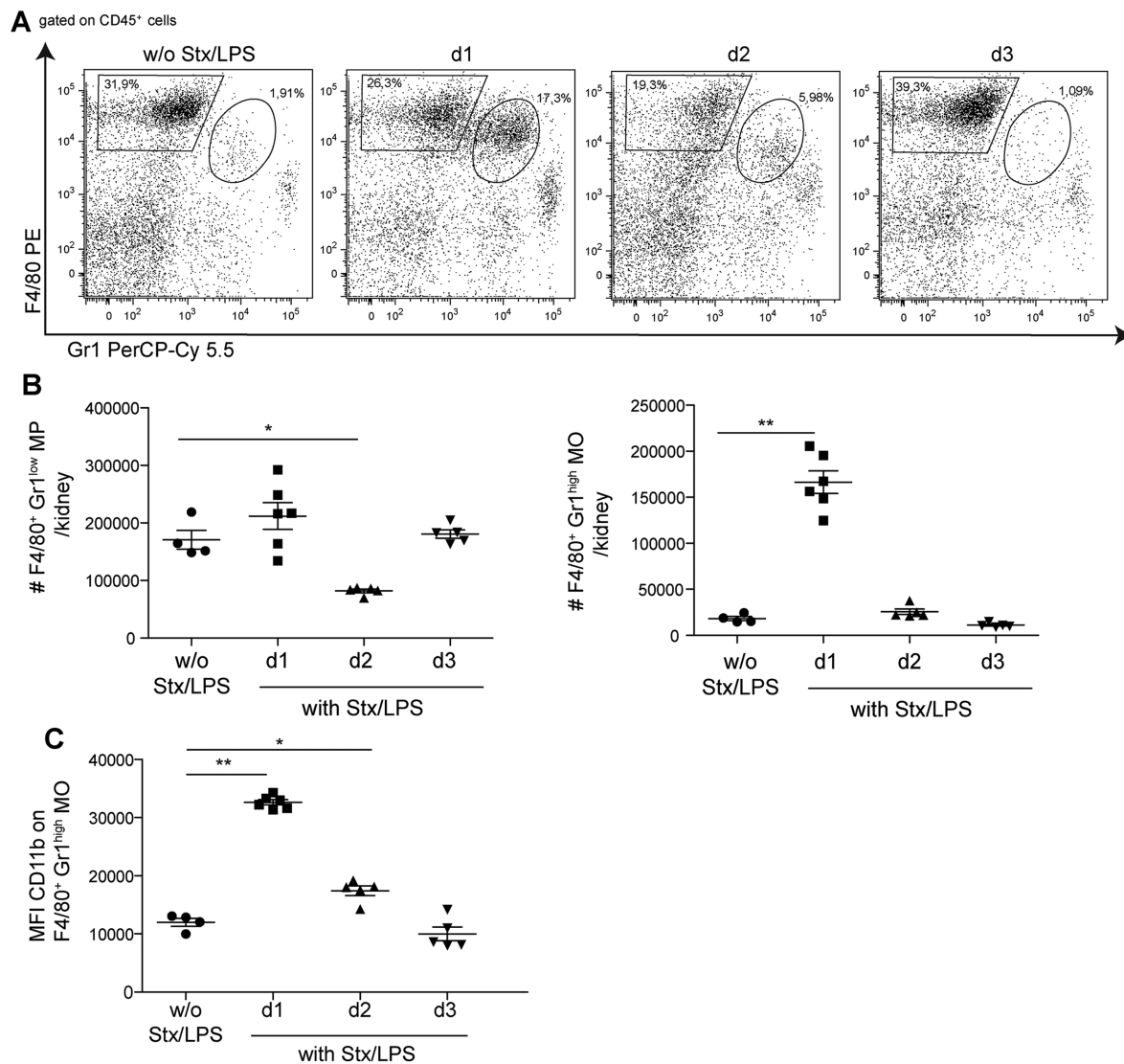


Figure 3. Increased abundance and activation of Gr1^{high} monocytes in the kidney of Stx/LPS-injected mice. (A) Representative FACS plot of renal leukocytes (gated on CD45⁺ cells) stained for F4/80 and Gr1 on day 1 to day 3 after Stx/LPS injection. (B) Absolute numbers of Gr1^{low} macrophages (F4/80⁺Gr1^{low}) and Gr1^{high} monocytes (F4/80⁺Gr1^{high}), pregated on CD45⁺ leukocytes, were analyzed on day 1 to day 3 after Stx/LPS injection by flow cytometry. (C) MFI of CD11b staining on Gr1^{high} monocytes in the kidney of Stx/LPS-treated (with Stx/LPS) and control mice (w/o Stx/LPS). Data in (A) are representative of $n = 6-9$, which were generated in three independent experiments. Data in (B) are representative of three independent experiments. Data in (C) are from a single experiment with four to six mice. Results are given as mean \pm SEM and symbols represent a single mouse. p -value was calculated with Mann-Whitney test. * $p < 0.05$; ** $p < 0.01$. d = day; MFI = mean fluorescent intensity, MO = monocytes; MP = macrophages.

stimulation with Stx [34]. Notably, antibodies against CD11b are potent therapeutic agents in various diseases and targeting this integrin might serve as a potential therapy against HUS [35–37]. However, depletion of CD11b⁺ cells in CD11c DTR mice showed contrary results in the model of renal IRI [38, 39]. Moreover, depletion of these cells by clodronate- liposomes ameliorated renal damage [39]. These differential results might partially be explained by the efficacy of the depletion and the different myeloid cell types that are targeted by these approaches. These caveats have to be taken into consideration when analyzing the role of CD11b⁺ cells during HUS in a future study.

During HUS, activated Gr1^{high} monocytes may also exacerbate vascular damage in the glomerulus by producing pro-inflammatory molecules, such as TNF, which stimulate Gb3 synthesis and thereby leading to sensitization of endothelial cells to shiga toxin [40, 41]. We found reduced levels of the proinflammatory mediators IL-1b and IL-6 in mice deficient for CCR2 indicating that Gr1^{high} monocytes contribute to the inflammatory response during HUS. Conclusively, this study demonstrates the crucial role of CCR2-dependent Gr1^{high} monocytes during HUS. Targeting the recruitment of these cells to the kidney might serve as a therapy to reduce the kidney damage during HUS.

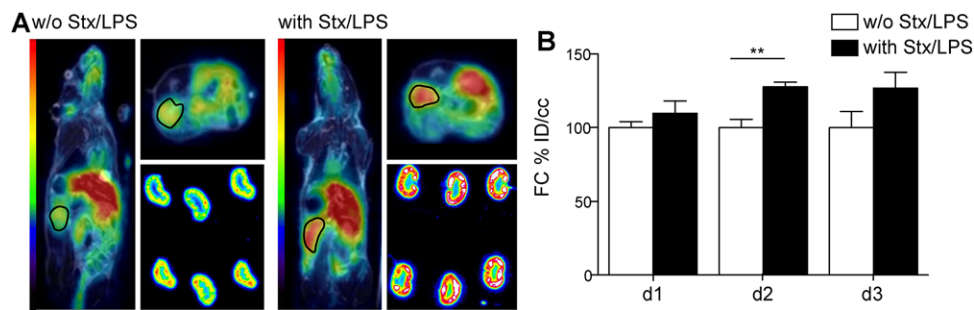


Figure 4. PET-MR imaging reveals increased kidney damage in the renal cortex. Mice were intravenously injected with Stx/LPS. One day later, the tracer [⁶⁴Cu]NOTA-GPVI-Fc was intravenously injected and the uptake in the kidney was assessed. (A) Representative in vivo PET-MR images (images on the left and upper right) of healthy control mice (w/o Stx/LPS) and two days after Stx/LPS injection (with Stx/LPS). Ex vivo autoradiography (images on the lower right with the six kidney slices) were analyzed in healthy controls and 3 days after Stx/LPS injection. (B) In vivo quantification of [⁶⁴Cu]NOTA-GPVI-Fc uptake in kidneys of untreated (w/o Stx/LPS, white bar) and Stx/LPS-treated mice (with Stx/LPS, black bar) on day 1 to day 3. The values are indicated as the mean of % injected dose (ID)/cc. Images and quantification (A) and (B) are representative of *n* = 3 (w/o Stx/LPS) and *n* = 5 (with Stx/LPS) from a single experiment. Results are given as mean ± SEM. *p*-value was calculated with Mann-Whitney test. ***p* < 0.01. FC = Fold change; %ID/cc = percentage injected dose per cubic centimeter; d = day.

Materials and methods

Mice

All mice were used between 7 and 14 weeks of age and backcrossed to a C57BL/6 background. Mice were bred and maintained under SPF conditions at the animal facilities of the University Clinic Essen and Bonn. *Ccr2*^{-/-} [42] mice were used to investigate the role of CCR2 during HUS. *Cx3cr1* *GFP*^{+/+} [43] mice were employed to determine the expression of the fractalkine receptor on monocytes and macrophages. Governmental review boards (Bezirksregierung Köln, Landesamt für Natur, Umwelt und Verbraucherschutz NRW in Recklinghausen, Germany) approved the mouse experiments.

Mouse model

The shiga toxin 2 (Stx) (Toxin Technology) dose were determined by a lethal challenge experiment by injecting serial dilutions of Stx in combination with a sublethal dose of LPS (56.25 ng/g mouse; Invivogen) in PBS intravenously into mice. The Stx dose that induces 100% mortality between 96 and 120 h (approximately 0.075 ng/g) was selected for the experiments.

Isolation of murine renal leukocytes

Renal leukocytes were isolated by cutting the kidneys into small pieces and digesting with 1 mg/mL collagenase and 0.1 mg/mL DNase-I (both from Sigma- Aldrich) in RPMI containing 10% FCS and 0.1% sodium azide. After an incubation period of 20 min at 37°C, kidneys were mashed with a syringe plunger and again incubated for 20 min at 37°C. Samples were homogenized by vigorously pipetting using 1000 µL tips and the supernatants were passed through a 100 µm nylon mesh.

BrdU incorporation assay

For in vivo labelling of proliferative cells, mice were intraperitoneally injected with 100 µL BrdU solution (10 mg/mL solution of BrdU in sterile 1 × DPBS) 1 day prior analysis. At the time points indicated, mice were sacrificed, kidneys were isolated and renal digests were processed for BrdU staining using the FITC BrdU Flow Kit by BD Biosciences according to the manufacturer's protocol.

Flow cytometry

For flow cytometric analysis murine cells were stained in the dark for 20 min at 4°C with following monoclonal antibody clones: CD115 (BV421 and PE, AFS98, BioLegend); CD11b (APC, M1/70, Biolegend); CD11c (APC-Cy7, HL3, BioLegend); CD45.1 (APC, A20, BD Biosciences); CD45 (BV421 and APC-Cy7, 30-F11, BioLegend); CD64 (PE/Cy7, X54-5/7.1, BioLegend); F4/80 (PE, BM8.1, Biolegend und APC, BM8.1, Tonbo Biosciences); Gr1 (PerCPcy5.5, RB6-8C5, Biolegend); Ly6C (PerCPcy5.5, HK1.4, BioLegend); Ly6G (FITC and BV421, 1A8, BioLegend); MerTK (PE, 2B10C42, BioLegend), MHC class II (PE-Cy7, M5/114.15.2, BioLegend); LIVE/DEAD™ Fixable Near-IR Dead Cell Stain Kit, for 633 or 635 nm excitation (Invitrogen). Unspecific Fc-receptor binding was blocked using human immune globulin (Privigen) diluted in PBS containing 1% FCS and 0.1% sodium azide. We determined absolute cell numbers by adding fixed numbers of CaliBRITE® APC-beads (6 µm) (BD Biosciences) before the flow cytometric measurement. Flow cytometry was performed on a BD LSR Fortessa II and data were analyzed with Flow-Jo® software (Tristar).

Serum analysis

Blood of Stx/LPS-injected mice was obtained by cardiac puncture of the right heart chamber with a heparinized syringe containing 2 µL Heparin (5000 U/mL, Ratiopharm) in 28 µL PBS. The blood

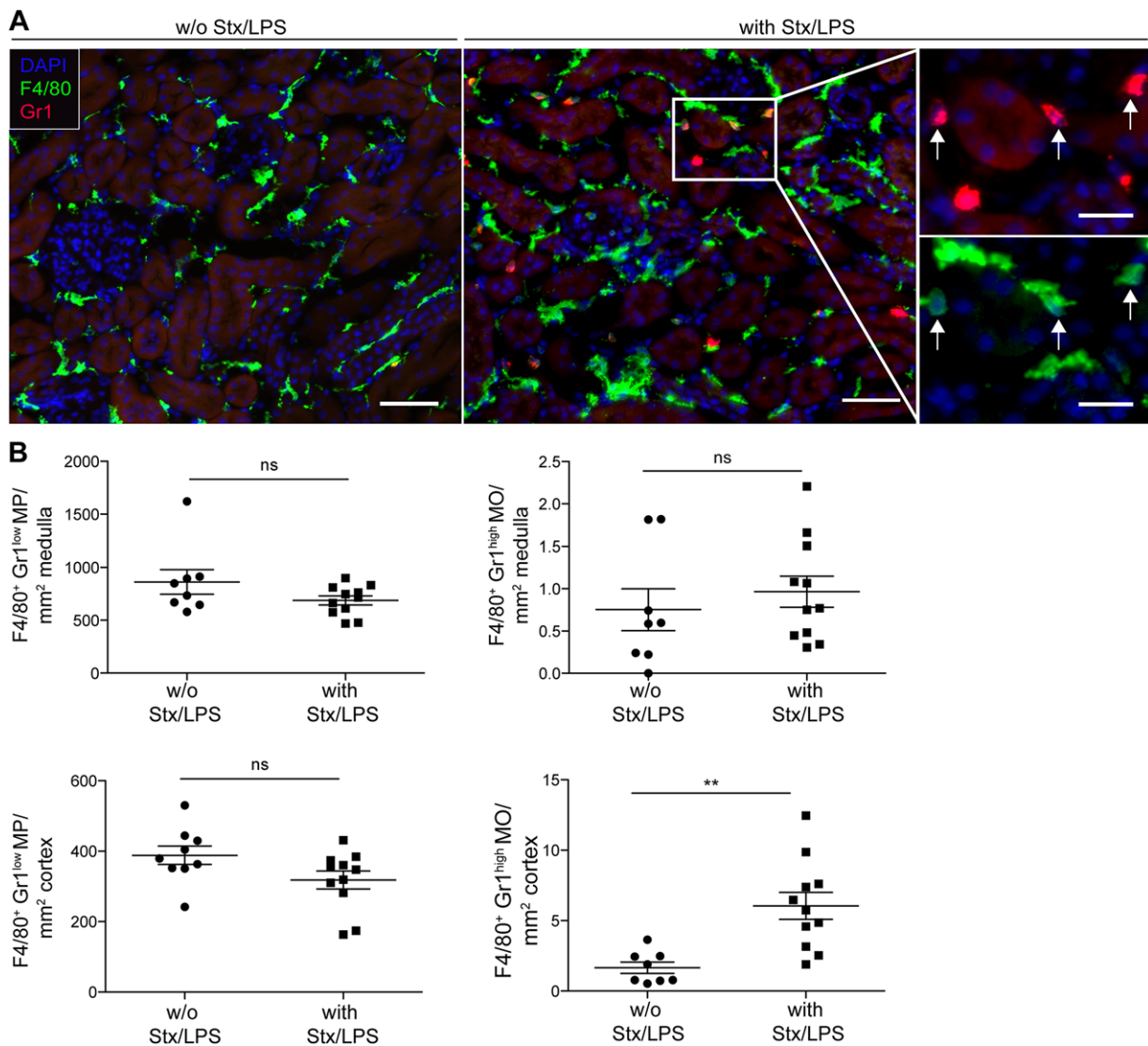


Figure 5. Gr1^{high} monocytes localize within the renal cortex. (A) Representative immunofluorescent images from kidneys of untreated mice (w/o Stx/LPS) and one day after Stx/LPS injection. Cryosections (10 µm) were stained with Gr1 (red) and F4/80 (green) antibody. The nucleus was stained by DAPI (dark-blue). Arrows indicate Gr1^{high} monocytes (F4/80⁺Gr1^{high}). The white bar indicates 50 µm (overview images) and 20 µm (zoom images). (B) The number of Gr1^{low} macrophages (F4/80⁺Gr1^{low}) (left scatter plots) and Gr1^{high} monocytes (F4/80⁺Gr1^{high}) (right scatter plots) in the medulla (upper scatter plots) and in the renal cortex (lower scatter plots) were determined in healthy control mice (w/o Stx/LPS) and 1 day after Stx/LPS injection. The images in (A) and the analysis in (B) are representative of $n = 9$ (w/o Stx/LPS) and $n = 11$ (with Stx/LPS) mice from three independent experiments. Results are given as mean \pm SEM and symbols represent a single mouse. p -value was calculated with unpaired t -test. ** $p < 0.01$. MO = monocytes, MP = macrophages.

was centrifuged at $16\,000 \times g$ for 10 min at 4°C to measure the BUN levels in the plasma.

KIM-1 expression by RT-PCR

Whole-tissue RNA from kidneys was extracted using NucleoSpin RNA plus kit (Macherey-Nagel), according to the manufacturer's instructions. RNA was reverse transcribed into cDNA using QuantiTect Reverse Transcription Kit (Qiagen). Quantitative PCR was performed for 40 cycles using QuantiFast SYBR Green PCR Kit (Qiagen). To detect mouse gene expression of KIM-1 following primers were used (Mm *havr1* fwd:

5'-TCCTGAGGATGTCACAGTGC-3, Mm *havr1* rev: 5'-CACAC ATGGACTCACAACCA-3'). All samples were measured in duplicates and normalized to *hprt* primers (fwd: 5'-GTCCAGCGTC GTGATTAGCGAT-3'; rev: 5'-GGGCCACAATGTGATGGCCTCC-3').

Adoptive transfer of CD45.1⁺ Gr1^{high} monocytes

To adoptively transfer bone-marrow-derived Gr1^{high} monocytes, bone marrow cells from tibia and femur of CD45.1 donor mice were isolated. Then, a two-step MACS isolation procedure was established: first, monocytes were negatively selected from the cell suspension using the Monocyte Isolation Kit (Miltenyi Biotec).

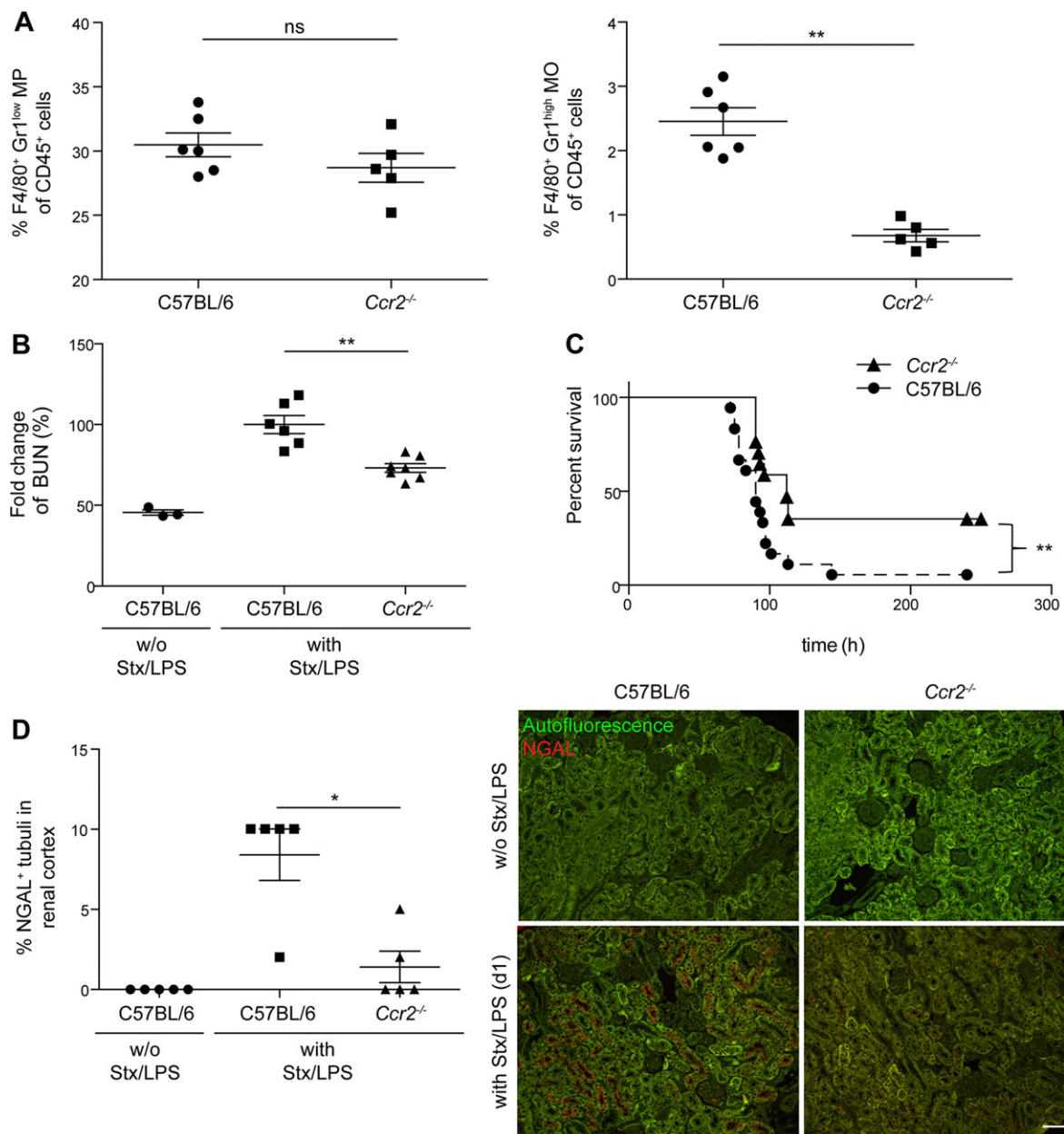


Figure 6. Reduced abundance of Gr1^{high} monocytes ameliorates kidney injury in *Ccr2*^{-/-} mice. (A) Frequencies of Gr1^{low} macrophages (left panel) and Gr1^{high} monocytes (right panel) in the kidney of C57BL/6 and *Ccr2*^{-/-} mice at the time point of Stx/LPS injection (day 0). (B) Fold change of BUN levels in the plasma 3 days after Stx/LPS injection in C57BL/6 and *Ccr2*^{-/-} mice. (C) Survival of C57BL/6 (circles, dashed line) and *Ccr2*^{-/-} mice (triangles, solid line) injected with Stx/LPS. (D) The expression of NGAL in C57BL/6 and *Ccr2*^{-/-} mice was determined by histology at d1 post Stx/LPS treatment and compared to untreated mice. Histological sections were stained with an NGAL antibody and the percentage of NGAL⁺ tubuli in the renal cortex were determined. Data in (A) and (B) are representative of two independent experiments with three to seven mice per group. Survival curve in (C) represents $n = 18$ (C57BL/6) and $n = 15$ (*Ccr2*^{-/-}) from three independent experiments. Data in (D) represent a single experiment with $n = 5$ mice. Results are given as mean \pm SEM. p -values in A, B and D were calculated with Mann-Whitney test. p -value in C was calculated with Log-Rank (Mantel-Cox) test. * $p < 0.05$; ** $p < 0.01$. MO = monocytes; MP = macrophages; BUN = blood urea nitrogen; NGAL = neutrophil gelatinase-associated lipocalin.

Next, Gr1^{high} monocytes were enriched by a positive selection step using a biotinylated Ly6C antibody and Streptavidin MicroBeads (Miltenyi Biotec). A purity of 80% was achieved. A total number of 1.4×10^6 Gr1^{high} monocytes were adoptively transferred into CD45.2 recipient mice by intravenous injection 3.5 h post Stx/LPS injection.

Chemokine/cytokine analysis

In the supernatant of mechanically homogenized murine kidneys the protein levels of chemokines were determined by using the flow-cytometry based beads assay LEGENDplexTM Mouse Proinflammatory Chemokine Panel

(13-plex) according to the manufacturer's protocol (BioLegend).

In vivo PET Imaging

High-resolution non-invasive in vivo PET images were acquired using two small animal Inveon microPET scanners (Siemens Medical Solutions USA, Inc., Knoxville, TN, USA) with a transaxial field of view (FOV) of 10 cm, and an axial FOV of 12.7 cm and a spatial resolution of 1.5 mm in the reconstructed PET images.

Mice were anesthetized with 1.5% isoflurane-O₂ (1.5 l/min, 1.5% isoflurane, Abbott GmbH, Wiesbaden, Germany) and injected intravenously with 9.5 ± 0.9 MBq [⁶⁴Cu]NOTA-GPVI-Fc tracer 24 h after Stx/LPS injection. Static PET acquisitions were performed under isoflurane anesthesia, after an uptake time of 60 min, 24 h and 48 h after tracer injection. During PET scans, mice were placed on a heating mat (37°C) to maintain body temperature.

For reconstruction of the PET images, list mode data were processed applying the statistical iterative ordered subset expectation maximization (OSEM) 2D algorithm.

All data were corrected for decay and normalized for each animal to the injected activity. Data were analyzed by drawing regions of interests around the whole left kidney of each mouse. The right kidney was not analyzed to exclude false positive values caused by spillover effects from the unspecific signal in the liver. Image analysis was performed with the Pmod Software (Pmod Technologies Ltd., Zurich, Switzerland).

In vivo MR Imaging

MRI was performed using a 7 T small-animal scanner (Biospec, Bruker Biospin MRI GmbH, Ettlingen, Germany). All mice were anesthetized with 1.5 vol% isoflurane and placed within the scanner's FOV. Imaging was performed using a 3D TurboRARE (TE/TR 58/1800 ms) sequence.

Ex vivo autoradiography

To perform autoradiography, animals were injected with 9.5 ± 0.9 MBq [⁶⁴Cu]NOTA-GPVI-Fc tracer 24 h after Stx/LPS injection. A total of 72 h after Stx/LPS injection, mice were sacrificed and kidneys were removed and embedded in a cutting compound (TissueTek; Sakura Finetek, Torrance, CA, USA). Autoradiography was performed on 20 μm kidney slices with a Storage Phosphor Screen (Molecular Dynamics, Sunnyvale, CA, USA). After an exposure time of 24 h, the phosphor screen was scanned at a resolution of 50 μm/pixel with a STORM Phosphor-Imager (Molecular Dynamics).

Immunohistochemistry

A total of 10 min before sacrificing the mice 2 μg of the Gr-1 antibody (PE, RB6-8C5, BD Bioscience) were injected intravenously.

Kidneys were isolated 24 h after Stx/LPS injection and fixed with 0.05 M phosphate buffer containing 0.1 M L-lysine (pH 7.4, Roth), 2 mg/mL NaIO₄ (Roth), and 10 mg/mL paraformaldehyde (Sigma-Aldrich) overnight at 4°C. Kidneys were equilibrated in 30% sucrose (Roth) solution for 24h. Tissues were then frozen in OCT (Weckert Labortechnik) and stored at –80°C. Consecutive sections (10 μm) were mounted on Super Frost Plus glass slides (R.Langenbrinck), dried for 10 min at 70°C, rehydrated with PBS with 0.05% Triton X-100 (Roth) and blocked for 1 h with PBS containing 1% bovine serum albumin (GE Healthcare) and 0.05% Triton X-100. The staining was performed in blocking buffer (200 μL volume per section). The F4/80 antibody (APC, BM8.1, Tonbo bioscience, dilution of 1:100) was incubated for 1 h, DAPI (2 mg/mL, Life Technologies, diluted 1:5000) was incubated for 5 min. After each staining step, three washing steps of 5 min with 0.05% Triton X-100 in PBS were performed. Sections were imaged by the Zeiss Axio Observer.Z1 and Apotome (Zeiss) at the Imaging Center Essen and analysed by the ZEN Software (Zeiss) and FIJI.

To determine NGAL, mice were sacrificed, renal tissue were dissected, fixed in 4% paraformaldehyde (PFA) and embedded in paraffin. Sections (2 μm) were cut and stained for NGAL (rat anti-mouse, Dianova, dilution of 1:1000) to detect tubular damage. Trypsin digest for 15 min at 37°C or by incubation in citrate buffer in the microwave (15 min at 600 Watt) was used for antigen retrieval. After incubation with primary antibodies for 60 min at room temperature in the dark Alexa Fluor conjugated secondary antibodies (488) were incubated for additional 60 min. Analysis was performed in a blinded manner using a Leica imaging microscope. To assess tubular damage, the percentage of tubuli with NGAL expression was estimated in ten different view fields of the cortex in 200-fold magnification.

Total kidney images were generated by the Keyence microscope software with stack function. All images were captured with the same window size.

Statistical analysis

Appropriate assumptions of data (normal distribution or similar variation between experimental groups) were examined before statistical tests were conducted. The sample size was analyzed by G*Power analysis to ensure adequate power to detect a pre-specified effect size. The numbers of mice per group are given in the Figure legends. Comparisons were made using non-parametric Mann–Whitney or two-tailed *t*-test. Comparison of survival curves was performed using a Log-rank (Mantel-Cox) test. Results are expressed as mean ± SEM, **p* < 0.05; ***p* < 0.01; ****p* < 0.001.

Acknowledgements: The authors acknowledge support by the Animal Facilities, the Imaging Core Facility (IMCES), the Institute of Immunology, the Department of Endocrinology and

Metabolism, Division of laboratory research at the University Hospital Essen and Anke Carstensen from the Institute of clinical chemistry and pharmacology, University Hospital Bonn. This work was supported by grants of The Deutsche Forschungsgemeinschaft (KFO274, EN984/1-1, EN984/5-1, EN984/6-1 and SFBTR57), the Marga und Walter-Boll Stiftung, MERCUR and intramural funding by the Medical Faculty of the University Duisburg-Essen (IFORES). We thank Prof. Dr. Meinrad Gawaz, Department of Internal Medicine III, University of Tuebingen for providing GPVI-Fc.

Conflict of interest: The authors declare no commercial or financial conflict of interest.

References

- Tarr, P. I., Gordon, C. A. and Chandler, W. L., Shiga-toxin-producing *Escherichia coli* and haemolytic uraemic syndrome. *Lancet* 2005. **365**: 1073–1086.
- Sandvig, K. and Van Deurs, B., Endocytosis, intracellular transport, and cytotoxic action of Shiga toxin and ricin. *Physiol. Rev.* 1996. **76**: 949–966.
- Palermo, M. S., Alves Rosa, M. F., van Rooijen, N. and Isturiz, M. A., Depletion of liver and splenic macrophages reduces the lethality of Shiga toxin-2 in a mouse model. *Clinical Experimental Immunol.* 1999. **116**: 462–467.
- Keepers, T. R., Psotka, M. A., Gross, L. K. and Obrig, T. G., A murine model of HUS: Shiga toxin with lipopolysaccharide mimics the renal damage and physiologic response of human disease. *J. Am. Soc. Nephrol.* 2006. **17**: 3404–3414.
- Keepers, T. R., Gross, L. K. and Obrig, T. G., Monocyte chemoattractant protein 1, macrophage inflammatory protein 1 α , and RANTES recruit macrophages to the kidney in a mouse model of hemolytic-uremic syndrome. *Infect. Immun.* 2007. **75**: 1229–1236.
- Locatelli, M., Buelli, S., Pezzotta, A., Corna, D., Perico, L., Tomasoni, S., Rottoli, D. et al., Shiga toxin promotes podocyte injury in experimental hemolytic uraemic syndrome via activation of the alternative pathway of complement. *J. Am. Soc. Nephrol.* 2014. **25**: 1786–1798.
- Menon, M. C., Chuang, P. Y. and He, C. J., The glomerular filtration barrier: components and crosstalk. *Internat. J. Nephrol.* 2012. **2012**: 749010.
- Obrig, T. G. and Karpman, D., *Shiga toxin pathogenesis: kidney complications and renal failure Ricin and Shiga toxins*. Springer, 2011, pp 105–136.
- O'Loughlin, E. V. and Robins-Browne, R. M., Effect of Shiga toxin and Shiga-like toxins on eukaryotic cells. *Microbes Infect.* 2001. **3**: 493–507.
- Harrison, L. M., Cherla, R. P., van den Hoogen, C., van Haften, W. C., Lee, S. Y. and Tesh, V. L., Comparative evaluation of apoptosis induced by Shiga toxin 1 and/or lipopolysaccharides in human monocytic and macrophage-like cells. *Microb. Pathog.* 2005. **38**: 63–76.
- Soos, T. J., Sims, T. N., Barisoni, L., Lin, K., Littman, D. R., Dustin, M. L. and Nelson, P. J., CX3CR1⁺ interstitial dendritic cells form a contiguous network throughout the entire kidney. *Kidney Int.* 2006. **70**: 591–596.
- Kurts, C., Panzer, U., Anders, H. J. and Rees, A. J., The immune system and kidney disease: basic concepts and clinical implications. *Nat. Rev. Immunol.* 2013. **13**: 738–753.
- Yang, N., Isbel, N. M., Nikolic-Paterson, D. J., Li, Y., Ye, R., Atkins, R. C. and Lan, H. Y., Local macrophage proliferation in human glomerulonephritis. *Kidney Int.* 1998. **54**: 143–151.
- Epelman, S., Lavine, K. J. and Randolph, G. J., Origin and functions of tissue macrophages. *Immunity* 2014. **41**: 21–35.
- Stamatiades, E. G., Tremblay, M.-E., Bohm, M., Crozet, L., Bisht, K., Kao, D., Coelho, C. et al., Immune monitoring of trans-endothelial transport by kidney-resident macrophages. *Cell* 2016. **166**: 991–1003.
- Serbina, N. V. and Pamer, E. G., Monocyte emigration from bone marrow during bacterial infection requires signals mediated by chemokine receptor CCR2. *Nat. Immunol.* 2006. **7**: 311–317.
- Zoja, C., Angioletti, S., Donadelli, R., Zanchi, C., Tomasoni, S., Binda, E., Imberti, B. et al., Shiga toxin-2 triggers endothelial leukocyte adhesion and transmigration via NF- κ B dependent up-regulation of IL-8 and MCP-1. *Kidney Int.* 2002. **62**: 846–856.
- van Setten, P. A., van Hinsbergh, V. W., van den Heuvel, L. P., Preyers, F., Dijkman, H. B., Assmann, K. J., van der Velden, T. J. et al., Monocyte chemoattractant protein-1 and interleukin-8 levels in urine and serum of patients with hemolytic uraemic syndrome. *Pediatr. Res.* 1998. **43**: 759–767.
- Ramos, M. V., Ruggieri, M., Panek, A. C., Mejias, M. P., Fernandez-Brando, R. J., Abrey-Recalde, M. J., Exeni, A. et al., Association of haemolytic uraemic syndrome with dysregulation of chemokine receptor expression in circulating monocytes. *Clin. Sci. (Lond.)* 2015. **129**: 235–244.
- Fernandez, G. C., Ramos, M. V., Gomez, S. A., Dran, G. I., Exeni, R., Alduncin, M., Grimoldi, I. et al., Differential expression of function-related antigens on blood monocytes in children with hemolytic uraemic syndrome. *J. Leukoc. Biol.* 2005. **78**: 853–861.
- Gawaz, M., Vogel, S., Pfannenbergh, C., Pichler, B., Langer, H. and Bigalke, B., Implications of glycoprotein VI for theranostics. *Thromb. Haemost.* 2014. **112**: 26–31.
- Bigalke, B., Pohlmeier, I., Schönberger, T., Griessinger, C. M., Ungerer, M., Botnar, R. M., Pichler, B. J. et al., Imaging of injured and atherosclerotic arteries in mice using fluorescence-labeled glycoprotein VI-Fc. *Eur. J. Radiol.* 2011. **79**: e63–e69.
- Rogers, B. E., Anderson, C. J., Connett, J. M., Guo, L. W., Edwards, W. B., Sherman, E. L., Zinn, K. R. et al., Comparison of four bifunctional chelates for radiolabeling monoclonal antibodies with copper radioisotopes: biodistribution and metabolism. *Bioconjug. Chem.* 1996. **7**: 511–522.
- Lim, J. K., Obara, C. J., Rivollier, A., Pletnev, A. G., Kelsall, B. L. and Murphy, P. M., Chemokine receptor Ccr2 is critical for monocyte accumulation and survival in West Nile virus encephalitis. *J. Immunol.* 2011. **186**: 471–478.
- Shi, C. and Pamer, E. G., Monocyte recruitment during infection and inflammation. *Nat. Rev. Immunol.* 2011. **11**: 762–774.
- Engel, D. R., Krause, T. A., Snelgrove, S. L., Thiebes, S., Hickey, M. J., Boor, P., Kitching, A. R. et al., CX3CR1 reduces kidney fibrosis by inhibiting local proliferation of profibrotic macrophages. *J. Immunol.* 2015. **194**: 1628–1638.
- Tang, X., Mo, C., Wang, Y., Wei, D. and Xiao, H., Anti-tumour strategies aiming to target tumour-associated macrophages. *Immunology* 2013. **138**: 93–104.
- Nywenning, T. M., Wang-Gillam, A., Sanford, D. E., Belt, B. A., Panni, R. Z., Cusworth, B. M., Toriola, A. T. et al., Targeting tumour-associated macrophages with CCR2 inhibition in combination with FOLFIRINOX in patients with borderline resectable and locally advanced pancreatic cancer: a single-centre, open-label, dose-finding, non-randomised, phase 1b trial. *Lancet Oncol.* 2016. **17**: 651–662.
- Zhang, J., Patel, L. and Pienta, K. J., Targeting chemokine (C-C motif) ligand 2 (CCL2) as an example of translation of cancer molecular biology to the clinic. *Prog. Mol. Biol. Transl. Sci.* 2010. **95**: 31–53.

- 30 Qian, B. Z., Li, J., Zhang, H., Kitamura, T., Zhang, J., Campion, L. R., Kaiser, E. A. et al., CCL2 recruits inflammatory monocytes to facilitate breast-tumour metastasis. *Nature* 2011. **475**: 222–225.
- 31 Vielhauer, V., Eis, V., Schlondorff, D. and Anders, H. J., Identifying chemokines as therapeutic targets in renal disease: lessons from antagonist studies and knockout mice. *Kidney Blood Press. Res.* 2004. **27**: 226–238.
- 32 Tsou, C. L., Peters, W., Si, Y., Slaymaker, S., Aslanian, A. M., Weisberg, S. P., Mack, M. et al., Critical roles for CCR2 and MCP-3 in monocyte mobilization from bone marrow and recruitment to inflammatory sites. *J. Clin. Invest.* 2007. **117**: 902–909.
- 33 Engel, D. R., Maurer, J., Tittel, A. P., Weisheit, C., Cavlar, T., Schumak, B., Limmer, A. et al., CCR2 mediates homeostatic and inflammatory release of Gr1^(high) monocytes from the bone marrow, but is dispensable for bladder infiltration in bacterial urinary tract infection. *J. Immunol.* 2008. **181**: 5579–5586.
- 34 Morigi, M., Galbusera, M., Binda, E., Imberti, B., Gastoldi, S., Remuzzi, A., Zoja, C. et al., Verotoxin-1-induced up-regulation of adhesive molecules renders microvascular endothelial cells thrombogenic at high shear stress. *Blood* 2001. **98**: 1828–1835.
- 35 Goodman, S. L. and Picard, M., Integrins as therapeutic targets. *Trends Pharmacol. Sci.* 2012. **33**: 405–412.
- 36 Duffield, J. S., Macrophages and immunologic inflammation of the kidney. *Semin. Nephrol.* 2010. **30**: 234–254.
- 37 Millard, M., Odde, S. and Neamati, N., Integrin targeted therapeutics. *Theranostics* 2011. **1**: 154–188.
- 38 Lin, S. L., Li, B., Rao, S., Yeo, E. J., Hudson, T. E., Nowlin, B. T., Pei, H. et al., Macrophage Wnt7b is critical for kidney repair and regeneration. *Proc Natl Acad Sci U S A* 2010. **107**: 4194–4199.
- 39 Ferenbach, D. A., Sheldrake, T. A., Dhaliwal, K., Kipari, T. M., Marson, L. P., Kluth, D. C. and Hughes, J., Macrophage/monocyte depletion by clodronate, but not diphtheria toxin, improves renal ischemia/reperfusion injury in mice. *Kidney Int.* 2012. **82**: 928–933.
- 40 Eisenhauer, P. B., Chaturvedi, P., Fine, R. E., Ritchie, A. J., Pober, J. S., Cleary, T. G. and Newburg, D. S., Tumor necrosis factor alpha increases human cerebral endothelial cell Gb3 and sensitivity to Shiga toxin. *Infect. Immun.* 2001. **69**: 1889–1894.
- 41 Stone, M. K., Kolling, G. L., Lindner, M. H. and Obrig, T. G., p38 mitogen-activated protein kinase mediates lipopolysaccharide and tumor necrosis factor alpha induction of shiga toxin 2 sensitivity in human umbilical vein endothelial cells. *Infect. Immun.* 2008. **76**: 1115–1121.
- 42 Kuziel, W. A., Morgan, S. J., Dawson, T. C., Griffin, S., Smithies, O., Ley, K. and Maeda, N., Severe reduction in leukocyte adhesion and monocyte extravasation in mice deficient in CC chemokine receptor 2. *Proc Natl Acad Sci USA* 1997. **94**: 12053–12058.
- 43 Jung, S., Aliberti, J., Graemmel, P., Sunshine, M. J., Kreutzberg, G. W., Sher, A. and Littman, D. R., Analysis of fractalkine receptor CX(3)CR1 function by targeted deletion and green fluorescent protein reporter gene insertion. *Mol. Cell. Biol.* 2000. **20**: 4106–4114.

Abbreviations: BUN: blood urea nitrogen · FOV: field of view · Gb3: globotriaosylceramide · GPVI: glycoprotein VI · HUS: hemolytic uremic syndrome · KIM-1: kidney injury marker-1 · MR: magnet resonance · NGAL: neutrophil gelatinase-associated lipocalin · OSEM: ordered subset expectation maximization · PET: positron emission tomography · PFA: paraformaldehyde · Stx: Shiga-Toxin

Full correspondence: Prof. Daniel R. Engel, Institute of Experimental Immunology and Imaging, University Duisburg-Essen, University Hospital Essen, 45147 Essen, Germany
e-mail: engel@immunodynamics.de

Received: 19/5/2017

Revised: 18/12/2017

Accepted: 5/2/2018

Accepted article online: 14/2/2018